Texture Analysis and Machine Learning for Detecting Myocardial Infarction in Noncontrast Low-Dose Computed Tomography: Unveiling the Invisible

Mannil, Manoj ; von Spiczak, Jochen ; Manka, Robert ; Alkadhi, Hatem

Abstract: OBJECTIVES The aim of this study was to test whether texture analysis and machine learning enable the detection of myocardial infarction (MI) on non-contrast-enhanced low radiation dose cardiac computed tomography (CCT) images. MATERIALS AND METHODS In this institutional review board-approved retrospective study, we included non-contrast-enhanced electrocardiography-gated low radiation dose CCT image data (effective dose, 0.5 mSv) acquired for the purpose of calcium scoring of 27 patients with acute MI (9 female patients; mean age, 60 ± 12 years), 30 patients with chronic MI (8 female patients; mean age, 68 ± 13 years), and in 30 subjects (9 female patients; mean age, 44 ± 6 years) without cardiac abnormality, hereafter termed controls. Texture analysis of the left ventricle was performed using free-hand regions of interest, and texture features were classified twice (Model I: controls versus acute MI versus chronic MI; Model II: controls versus acute and chronic MI). For both classifications, 6 commonly used machine learning classifiers were used: decision tree C4.5 (J48), k-nearest neighbors, locally weighted learning, RandomForest, sequential minimal optimization, and an artificial neural network employing deep learning. In addition, 2 blinded, independent readers visually assessed noncontrast CCT images for the presence or absence of MI. RESULTS In Model I, best classification results were obtained using the k-nearest neighbors classifier (sensitivity, 69%; specificity, 85%; false-positive rate, 0.15). In Model II, the best classification results were found with the locally weighted learning classification (sensitivity, 86%; specificity, 81%; false-positive rate, 0.19) with an area under the curve from receiver operating characteristics analysis of 0.78. In comparison, both readers were not able to identify MI in any of the noncontrast, low radiation dose CCT images. CONCLUSIONS This study indicates the ability of texture analysis and machine learning in detecting MI on noncontrast low radiation dose CCT images being not visible for the radiologists' eye.

DOI: https://doi.org/10.1097/RLI.0000000000000448

Texture Analysis and Machine Learning for Detecting Myocardial Infarction in Noncontrast Low-Dose Computed Tomography

Unveiling the Invisible

Manoj Mannil, MD, MSc, Jochen von Spiczak, MD, MSc,**
Robert Manka, MD,†‡ and Hatem Alkadhi, MD, MPH, EBCR**

Objectives: The aim of this study was to test whether texture analysis and machine learning enable the detection of myocardial infarction (MI) on non–contrast-enhanced low radiation dose cardiac computed tomography (CCT) images.

Materials and Methods: In this institutional review board–approved retrospective study, we included non–contrast-enhanced electrocardiography-gated low radiation dose CCT image data (effective dose, 0.5 mSv) acquired for the purpose of calcium scoring of 27 patients with acute MI (9 female patients; mean age, 60 ± 12 years), 30 patients with chronic MI (8 female patients; mean age, 68 ± 13 years), and in 30 subjects (9 female patients; mean age, 44 ± 6 years) without cardiac abnormality, hereafter termed *controls*. Texture analysis of the left ventricle was performed using free-hand regions of interest, and texture features were classified twice (Model I: controls versus acute MI versus chronic MI; Model II: controls versus acute and chronic MI). For both classifications, 6 commonly used machine learning classifiers were used: decision tree C4.5 (J48), k-nearest neighbors, locally weighted learning, RandomForest, sequential minimal optimization, and an artificial neural network employing deep learning. In addition, 2 blinded, independent readers visually assessed noncontrast CCT images for the presence or absence of MI.

Results: In Model I, best classification results were obtained using the k-nearest neighbors classifier (sensitivity, 69%; specificity, 85%; false-positive rate, 0.15). In Model II, the best classification results were found with the locally weighted learning classification (sensitivity, 86%; specificity, 81%; false-positive rate, 0.19) with an area under the curve from receiver operating characteristics analysis of 0.78. In comparison, both readers were not able to identify MI in any of the noncontrast, low radiation dose CCT images.

Conclusions: This study indicates the ability of texture analysis and machine learning in detecting MI on noncontrast low radiation dose CCT images being not visible for the radiologists' eye.

Key Words: texture analysis, myocardial infarction, machine learning, noncontrast, computed tomography

(*Invest Radiol* 2018;00: 00–00)

Computed tomography (CT) angiography enables the noninvasive detection of coronary atherosclerosis and obstructive coronary artery disease (CAD) with excellent test characteristics[1] and prognostic value.[2] In addition to the coronary arteries, CT has been tested also for identifying myocardial infarction (MI).[3] However, it was shown that CT has shortcomings for this indication as compared with the reference standard modality magnetic resonance (MR) imaging, mainly due to its limited contrast resolution and the relatively large amount of required intravenous contrast media (CM).[4]

Non–contrast-enhanced cardiac CT (CCT) images are usually performed for quantifying the calcium load of coronary arteries (so-called *calcium scoring*).[5] These noncontrast CCT images are acquired using electrocardiography (ECG)-gating and at low radiation doses.[6] Because of refraining from CM administration and applying low radiation doses, non–contrast-enhanced CCT images usually do not allow the diagnosis of cardiac abnormalities other than calcifications, which also includes the diagnosis of MI.[7]

Current advances in Radiomics enabled the translation of medical images into multidimensional data points.[8] In this regard, texture analysis (TA) objectively quantifies texture of radiological images by exploiting interpixel relationships.[9] These metrics can be used for diagnosing abnormalities in radiological images that cannot be seen by the radiologists' eyes alone.[10–13]

Interestingly, a recent study showed that certain TA features identified by machine learning allow the diagnosis of MI on non–contrast-enhanced cardiac cine MR images although no signal abnormalities could be visually demarcated.[14]

The purpose of this study was to test whether TA and machine learning enable the detection of MI on non–contrast-enhanced low radiation dose CCT images.

MATERIALS AND METHODS

Study Patients

Between February 2014 and June 2017, 87 patients (26 female patients, 61 male patients; mean age, 58 ± 14.5 years; range, 32–91 years) were included in this study: 27 patients with acute MI, 30 with chronic MI, and 30 showing no cardiac abnormalities (hereafter termed *controls*) (Table 1). Acute MI was defined as occurring less than 30 days after acute coronary syndrome, and chronic MI was defined as being older than 1 year since presentation.[15] All CCT examinations were clinically indicated.

Diagnosis of MI was mainly based on ECG findings, laboratory biomarkers, results from contrast-enhanced CCT (which was performed after nonenhanced CT), and to the results from catheter coronary angiography. Additional imaging modalities including MR imaging, single-photon emission CT, and positron emission tomography were used to aid image selection of patients with equivocal CT findings. Myocardial infarction extent was measured on contrast-enhanced CCT according to the 17-segment model of the American Heart Association.[16] Myocardial infarction was transmural in 6 (22%) of 27 acute MI patients and 14 (47%) of 30 chronic MI patients; subendocardial (<50% transmurality) in 21 (78%) of 27 acute MI patients and 16 (53%) of 30 chronic MI patients. The average extent of acute MI included 1.2 ± 0.6 myocardial segments; the average extent in chronic MI included 2.0 ± 0.8 segments.

Received for publication October 25, 2017; and accepted for publication, after revision, December 19, 2017.

From the *Institute of Diagnostic and Interventional Radiology, University Hospital Zurich, University of Zurich; †Institute for Biomedical Engineering, University and ETH Zurich; and ‡Department of Cardiology, University Heart Center, University Hospital Zurich, Zurich, Switzerland.

Correspondence to: Hatem Alkadhi, MD, MPH, EBCR, Institute of Diagnostic and Interventional Radiology, University Hospital Zurich, Raemistr. 100, CH-8091 Zurich, Switzerland. E-mail: hatem.alkadhi@usz.ch.

Supplemental digital contents are available for this article. Direct URL citations appear in the printed text and are provided in the HTML and PDF versions of this article on the journal's Web site (www.investigativeradiology.com).

ISSN: 0020-9996/18/0000–0000
DOI: 10.1097/RLI.0000000000000448

TABLE 1. Demographics of Controls and Patients With MI

Parameter	Controls	Patients With Acute MI	Patients With Chronic MI
n	30	27	30
Age, mean ± SD (range), y	44 ± 6 (32–55)	60 ± 12 (39–84)	68 ± 13 (44–91)
Sex	30% female 70% male	33% female 67% male	27% female 73% male
Agatston score, median ± IQR	0	101 ± 534	252 ± 1052
History of smoking	23%	63%	57%
Pack-years, mean ± SD, y	12 ± 2	39 ± 26	48 ± 27
Hypertension	7%	44%	60%
Hypercholesterolemia	7%	30%	50%
Diabetes	0%	22%	23%
Overweight (BMI > 30 kg/m^2)	3%	22%	20%

MI indicates myocardial infarction; BMI, body mass index; IQR, interquartile range; SD, standard deviation.

Controls showed no clinical or imaging evidence of CAD or other cardiac abnormalities. The indication for CCT in controls was atypical chest pain at a low pretest probability of CAD.

This retrospective study had institutional review board and local ethics committee approval; written informed consent requirement was waived.

CT Data Acquisition and Postprocessing

All examinations were performed on a second-generation dual-source CT scanner (SOMATOM Flash; Siemens Healthineers, Forchheim, Germany). The protocol consisted of a noncontrast followed by a contrast-enhanced CCT of the heart. Protocol and reconstruction parameters of contrast-enhanced CCT are not described in this manuscript because these data were not further analyzed in this study.

Acquisition parameters for non–contrast-enhanced CCT, performed for the purpose of calcium scoring, were as follows: slice collimation, 2 × 96 × 0.6 mm; slice acquisition, 2 × 192 × 0.6 mm using the *z*-flying focal spot; gantry rotation time, 250 milliseconds; reference tube voltage, 120 kVp; quality reference tube current-time product, 80 mA per rotation using automated exposure control (CAREDose, Siemens). Data acquisition was prospectively synchronized to the ECG in the high-pitch mode (pitch, 3.4). The average volume CT dose index was 1.32 ± 0.05 mGy; the average dose length product was 35.8 ± 5.5 mGy·cm; the average estimated effective radiation dose, using a conversion coefficient of 0.014,[17] was 0.5 ± 0.1 mSv.

Axial images of non–contrast-enhanced CCT were reconstructed with a slice thickness of 3 mm (increment, 3 mm) using a soft tissue convolution kernel (B35f). All images were anonymized and stored in digital imaging and communications in medicine (DICOM) file format for further processing.

Certain TA features require identical spatial resolution and pixel size to be comparable. Thus, all images were rescaled to a uniform in-plane resolution of 0.39 × 0.39 mm^2, representing a field of view of 200 × 200 mm^2 and a matrix size of 512 × 512, applying a custom MATLAB script (MathWorks, Natick).

Qualitative Visual Assessment

In patients with acute and chronic MI, those single axial images showing the largest extent of infarction on all available imaging studies including contrast-enhanced CCT were chosen. In controls, axial images through midventricular myocardial level were selected for qualitative visual assessment (Figs. 1, 2).

All non–contrast-enhanced CCT images were subjectively assessed by 2 independent readers (R1 and R2, with 2 and 4 years of experience in cardiovascular radiology, respectively) regarding the presence or absence of acute or chronic MI. Non–contrast-enhanced CCT images were presented at fixed window settings (width, 360; level, 70), and readers were allowed to change the settings according to their

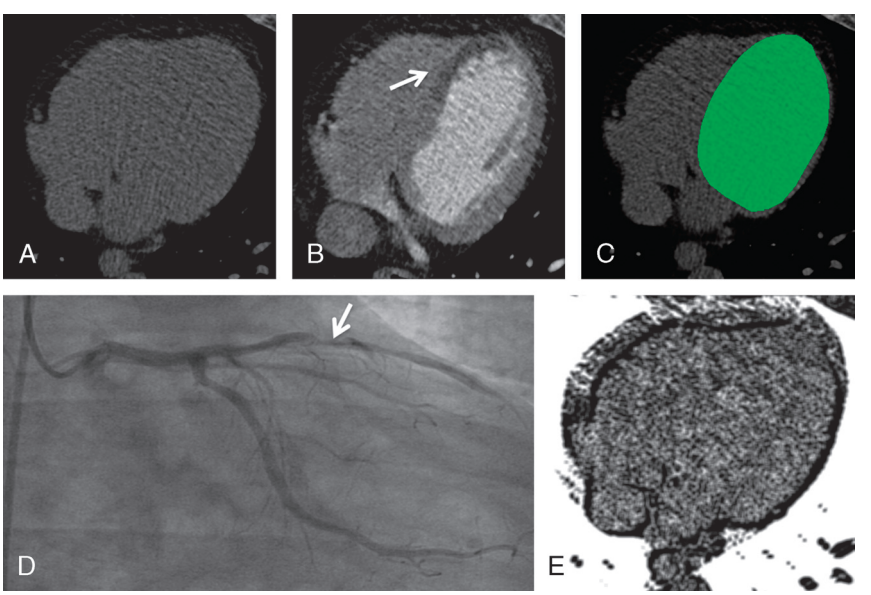

FIGURE 1. A–C, Axial CCT images of a 38-year-old male patient with acute myocardial infarction. A, The non–contrast-enhanced image shows no abnormalities; the infarct cannot be seen on these images. B, The contrast-enhanced image shows hypoattenuation of the midventricular and apical septum indicating infarction (arrow). C, Free-hand region of interest delineation (green) for texture analysis (TA) of the left ventricle including the blood pool on the non–contrast-enhanced CCT image. D, Catheter coronary angiography performed on the same day as CCT showed high-grade stenosis of the mid left anterior descending artery (arrow) and corresponding hypokinesia of the myocardium (not shown). E, Parametric map of the texture feature GLCM S5,-5 InvDfMom, which differed significantly between controls and patients with MI.

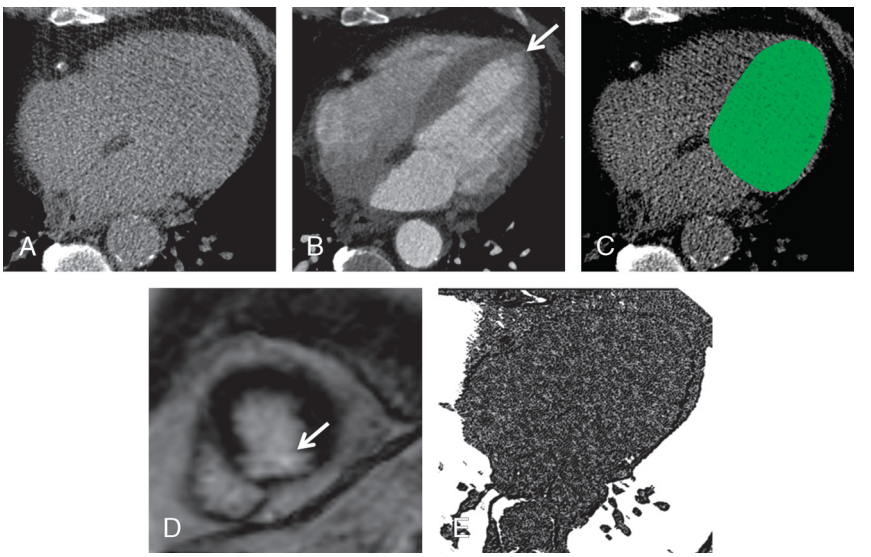

FIGURE 2. A and B, Axial CCT images of a 61-year-old male patient with chronic myocardial infarction. A, The non–contrast-enhanced image shows no abnormalities, the infarct cannot be seen. B, The contrast-enhanced image shows thinning of the left inferior apex (arrow), consistent with chronic scar. C, Free-hand region of interest delineation (green) for texture analysis (TA) of the left ventricle including the blood pool on the non–contrast-enhanced CCT image. D, Diagnosis was confirmed in short-axis cardiac MR image showing late gadolinium enhancement of the inferior apical myocardium (arrow). E, Parametric map of texture feature GLCM S5,-5 InvDfMom, which differed significantly between controls and patients with MI.

individual preferences. Both readers were blinded to patient information, to results of all other imaging tests (including contrast-enhanced CCT), and to the final diagnosis.

Texture Analysis

As recently shown by Sogawa et al,[18] TA was performed as a postprocessing step using noncommerical software (MaZda, version 4.6; Institute of Electronics, Technical University of Lodz, Lodz, Poland).[19] Gray level normalization was performed between the mean and 3 standard deviations ("±3σ" method) helping to correct for small technical variations.[20]

Similar to visual assessment, axial images showing the largest extent of infarction on contrast-enhanced CCT were used for TA in MI patients, whereas axial images at midventricular myocardial level were used in controls. Free-hand regions of interest (ROIs) of the myocardium and the blood pool were drawn on axial images by R1 and R2 for determining the interreader agreement of TA. R1 repeated ROI segmentation after 2 weeks for determining the intrareader agreement. Region of interest segmentation was performed side-to-side to contrast-enhanced CCT images and included both the left ventricular (LV) myocardium and the LV blood pool. The rationale was to minimize uncertainty in endocardial ROI delineation, especially in identifying the endocardial borders of the LV septum on non–contrast-enhanced CCT images (see Figs. 1, 2).

In total, 308 TA features were computed for each ROI originating from 6 main categories: (1) histogram (kurtosis, mean, skewness, variance), (2) gray-level co-occurrence matrix (GLCM) at 5 interpixel distances (angular second moment, contrast, correlation, difference entropy, difference variance, entropy, inverse different moment, sum average, sum entropy, sum of squares, sum variance), (3) run-length matrix at 4 angles: 180°, 135°, 90°, and 0° (fraction of image in runs, gray-level nonuniformity, long run emphasis, run-length nonuniformity, short run emphasis), (4) absolute gradient (gradient mean, kurtosis, non-zeros, skewness, and variance), (5) autoregressive model (Sigma and Teta 1–4,), and (6) wavelet transform (energy of wavelet coefficients in low-frequency sub-bands, horizontal high-frequency sub-bands, vertical high-frequency sub-bands, and diagonal high-frequency sub-bands).[19]

TA Feature Selection

Feature selection was performed on the 308 TA features. Hainc et al[9] recently showed the susceptibility of TA features to minor variation in ROI delineation. Therefore, all feature pairs showing a reduced intrareader and interreader agreement according to calculated intraclass correlation coefficients (ICCs) were removed from further analysis. Landis and Koch interpreted ICCs of 0.61 to 0.8 as substantial and 0.81 to 1.00 as excellent agreement.[21] Thus, we excluded TA features with ICC ≤ 0.6 from further analyses. To enhance classification results further, we used an attribute-selected classifier with built-in capabilities to evaluate the worth of a subset of attributes with dedicated machine learning software (Weka, University of Waikato, Waikato, New Zealand). The classifier considered the individual predictive ability of each TA feature and the degree of redundancy between them in the training data set.

Statistical Analysis

Categorical variables were provided as percentages or frequencies. Continuous variables were expressed as medians with interquartile ranges (IQRs) or means ± standard deviation. The qualitative visual analysis regarding the detection of MI was compared with the reference standard. The intrareader and interreader agreement for qualitative visual analysis was calculated using Cohen's κ.

For quantitative image classification, we used 2 models: In Model I, we analyzed the predictive classification of selected TA features in correctly identifying controls, acute MI, and chronic MI. In Model II, we pooled acute and chronic MI and tested the classification of cases versus controls. In both approaches, we tested 6 machine learning classifiers commonly used in recent literature[22–24]: decision tree C4.5 (J48), k-nearest neighbors (k-NN) (k = 1–6), locally weighted learning (LWL), RandomForest, sequential minimal optimization (SMO), and deep learning facilitated by an artificial neural network with backpropagation (Epoch = 500; learning rate = 0.3; momentum = 0.2).

To account for overfitting, we split the data set in the recommended ratio of two thirds for training and one third for testing.[25] Obtained results of the 6 machine learning-based classifiers were compared regarding sensitivity, specificity, and area under the curve (AUC) from receiver operating characteristics analysis. Normal

distribution was tested by means of a Shapiro–Wilk test. Differences among single TA features between cases and controls were compared using a Mann–Whitney *U* Test. Statistical significance was defined by a 2-tailed *P* value below 0.05. To account for multiple comparisons, Bonferroni correction was applied when required. Machine learning classifications were computed using noncommercial software (WEKA, University of Waikato, Waikato, New Zealand), all remaining statistical analyses were conducted using commercial software (SPSS 23.0; IBM, Chicago, Ill).

RESULTS

Qualitative Visual Analysis

Subjective visual differentiation of controls as well as acute and chronic MI cases on non–contrast-enhanced CCT images was not possible in any of the 57 patients and 30 controls for either of the 2 readers R1 and R2 ($\kappa = 1$). Two representative examples of patients with acute and chronic MI are depicted in Figures 1 and 2.

Dimension Reduction

After excluding 232 of the 308 TA features (75%) because of reduced ICCs, 76 features (25%) remained for further analysis. Of these, 84% showed substantial and 16% excellent interreader and intrareader agreement. These remaining features showed on average substantial interreader (ICC, 0.75 ± 0.1; range, 0.6–0.99) and excellent intrareader agreement (ICC, 0.86 ± 0.1; range, 0.72–0.98) (Supplementary Table 1, Supplemental Digital Content, http://links.lww.com/RLI/A369). Attribute selected classifier-based dimension reduction improved outcome classification only in Model II, where it returned 3 TA features: GLCM S5,-5InvDfMom, Teta2, and Teta3.

Model I: Controls Versus Acute MI Versus Chronic MI

For differentiation between controls (n = 30), acute MI (n = 27), and chronic MI (n = 30), all 6 classifiers provided high to near-perfect classification results based on the training data set. On the test data set, best results were obtained using the k-NN classifier algorithm with k = 1 and a brute force search algorithm utilizing the Euclidean Distance.[26] In this setting, 69% of the test data were correctly classified with a sensitivity of 72.7% for controls, 71.4% for patients with acute MI, and 63.6% for patients with chronic MI. The overall specificity was 85%, the specificity for healthy controls was 77.8%, the specificity for patients with acute MI was 81.8%, and the specificity for patients with chronic MI was 94.4%. Receiver operating characteristics analysis revealed an AUC of 0.77 (controls: AUC = 0.75; acute MI: 0.77; chronic MI: AUC = 0.79) for differentiating controls versus patients with acute MI versus patients with chronic MI (Table 2).

Model II: Controls Versus Patients With MI

For differentiation between controls (n = 30) and patients with both acute and chronic MI (n = 57), dimension reduction yielded 3 TA features (GLCM S5,-5InvDfMom, Teta2, and Teta3) enabling the differentiation between the 2 groups (Fig. 3).

Based on the training data set, all 6 classifiers provided high to near-perfect classification results. Overall best classification results on the test data set were obtained by use of LWL based on the decision stump classifier and a brute force search algorithm utilizing the Manhattan distance.[27] In this setting, 86.2% of test data could be correctly classified. Sensitivity was 72.7% for healthy controls and 94.4% for patients with acute or chronic MI. Overall specificity was 81%, with a specificity of 94.4% for healthy controls and 72.7% for patients with acute or chronic MI. Receiver operating characteristics revealed an AUC of 0.78 for differentiating controls versus cases (controls: AUC = 0.78; cases: AUC = 0.78) (see Table 2).

DISCUSSION

This proof-of-concept study indicates that certain TA features combined with machine learning algorithms enable the differentiation between controls and patients with acute or chronic MI on non–contrast-enhanced low radiation dose CCT images with high accuracy, hereby unveiling image information that is not visible to the radiologists' eye. Gosalia et al[4] were among the first to describe the potential of contrast-enhanced chest CT for detecting MI. Later studies using ECG-gated acquisitions in the first-pass arterial phase confirmed the ability of CCT to diagnose MI.[3] To the best of our knowledge, no study so far has used non–contrast-enhanced CCT images for detecting MI. The ability to detect MI on non–contrast-enhanced CCT images would be advantageous concerning patient safety and costs. Especially in light of the increasing prevalence of allergies, the omission of CM would be an asset. Moreover, identification of MI on non–contrast-enhanced CCT images performed for calcium scoring would indicate that further contrast-enhanced coronary CT angiography is not appropriate due to the high pretest probability of CAD[28] and the then reduced test characteristics.[1]

TABLE 2. Detailed Results of the Machine Learning-Based Classification of Texture Analysis Features

Classification	Classifier	Correctly Classified Instances, %	Sensitivity*	Specificity*	AUC
Controls vs acute MI vs chronic MI	C4.5	48.3	0.48	0.73	0.61
	Deep learning	51.7	0.52	0.79	0.71
	k-NN	**69.0**	**0.69**	**0.85**	**0.77**
	LWL	41.4	0.41	0.36	0.61
	RandomForest	51.5	0.52	0.78	0.61
	SMO	51.7	0.52	0.77	0.71
Controls vs patients (acute and chronic MI)	C4.5	75.9	0.76	0.64	0.67
	Deep learning	75.9	0.76	0.64	0.7
	k-NN	62.1	0.62	0.52	0.57
	LWL	**86.2**	**0.86**	**0.81**	**0.78**
	RandomForest	**79.3**	0.79	0.73	0.82
	SMO	62.1	0.62	0.38	0.5

Best classifications are indicated in boldface.

*Weighted average.

AUC indicates area under the curve; k-NN, k nearest neighbors; LWL, locally weighted learning; MI, myocardial infarction; SMO, sequential minimal optimization.

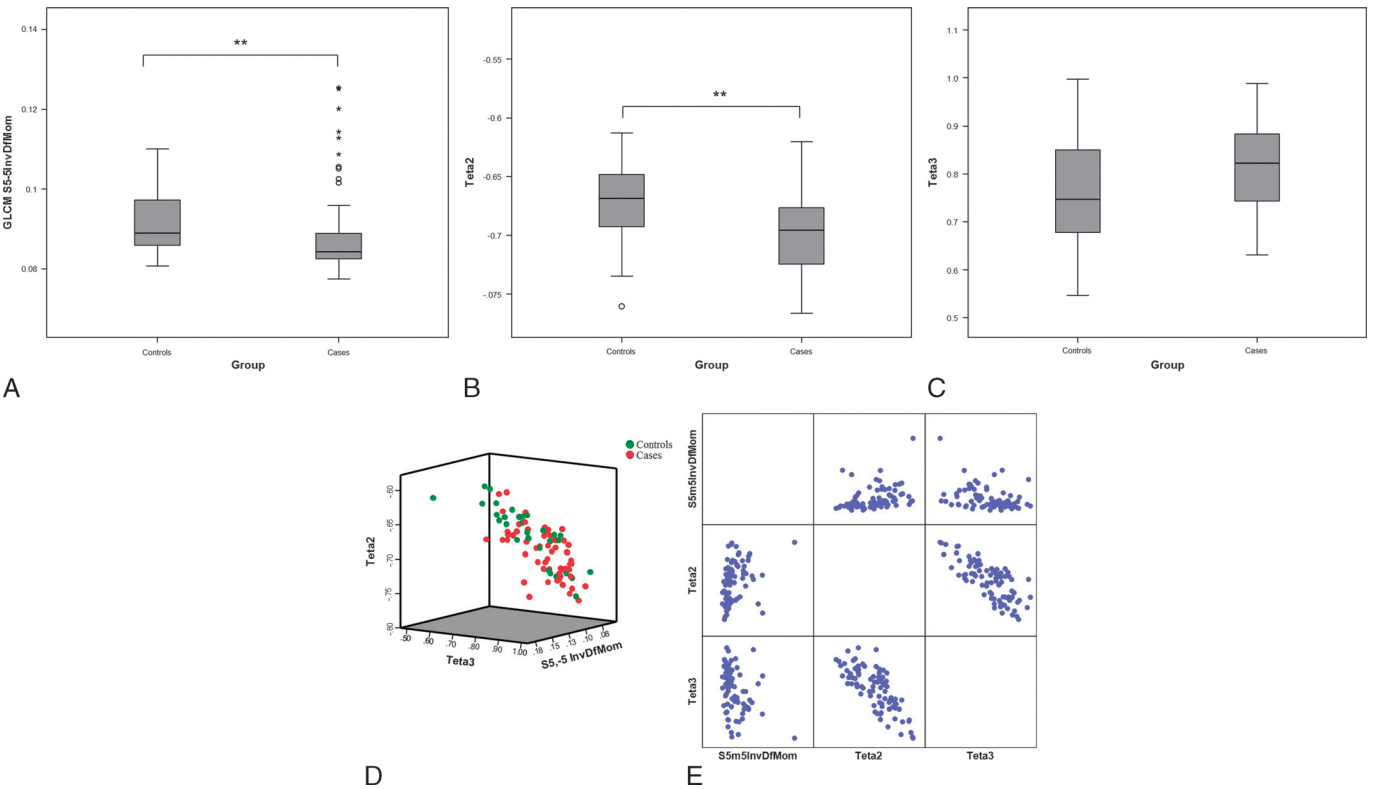

FIGURE 3. A–C, Comparison of controls and cases (pooled acute and chronic MI) of selected TA features after dimension reduction: (A) GLCM feature S5,-5InvDfMom ($P = 0.009$), (B) autoregressive model feature Teta2 ($P = 0.002$), and (C) autoregressive model feature Teta3 ($P = 0.043$). Statistical significance indicated by 2 asterisks (**). D, Three-dimensional scatterplot of TA features GLCM S5,-5InvDfMom, Teta2, and Teta3 visualized in the feature space indicating the differentiation between patients with MI (red) and controls (green) by means of lower GLCM S5,-5 InvDfMom, lower Teta2, and higher Teta3 values. E, Correlation matrix of the 3 TA features (dimensionless) demonstrating an inverse correlation between Teta2 and Teta3.

Our results showed moderate accuracy for differentiating between controls versus patients with acute MI versus patients with chronic MI. However, we found marked improvements in accuracy when pooling patients with both acute and chronic MI, showing a classification accuracy of 86%, a sensitivity of 86%, specificity of 81%, and an AUC of 0.78. This differentiation between controls and patients with infarcts was not possible by visual assessment of 2 readers being experienced in cardiovascular imaging.

The improved result for pooled patients suggest certain overlap of texture features in infarcts of different age. Still, the classification between healthy and diseased heart was accurate despite of the relatively low number of patients included, the low radiation dose of the protocol (0.5 mSv) resulting in high noise levels, and the potential inaccuracies in ROI segmentation of the LV borders including also the LV blood pool. Thus, results from TA in combination with machine learning can be expected to be even more accurate when including more patients, using a higher dose protocol, and when improving the precision of ROI segmentation.

A common problem in machine learning-based analyses is overfitting of data.[25] To avoid a perfect classification custom tailored to the present data set, a recommended two thirds of data were used for training and decision tree generation. The remaining third was used for model validation.[25] Group allocation was performed by random. However, within the training and test data sets controls and cases were distributed in a balanced fashion. There are several approaches toward dimension reduction.[29] We assessed the individual predictive ability of each TA feature along with the degree of redundancy. Furthermore, we excluded TA features with compromised reproducibility. Future automated segmentation tools may render this step redundant as recently suggested by Depeursinge et al.[30]

Classifications for differentiation between controls and patients with both acute and chronic MI were based on a combination of 3 single TA features: GLCM S5,-5InvDfMom, Teta2, and Teta3, while no first-level histogram feature such as, for example, the average or skewness of attenuation remained in the model after feature reduction. The GLCM inverse difference moment (InvDfMom) feature measures image homogeneity. Its value is reciprocal to gray tone differences in pair elements. Our results show significantly higher InvDfMom/homogeneity values for controls than for patients with MI, implying higher gray tone differences for cases than for controls. The 2 remaining TA features Teta2 and Teta3 are derived from the autoregressive model.[31] This model assumes a local interaction between pixels and describes each pixel gray value as a weighted sum of adjacent pixel values. For coarse textures, the coefficients of neighboring pixels are similar to each other, while for fine textures the coefficients vary more widely. Since 2 of the total 4 Teta features (Teta1 – Teta4) differ significantly and contribute to model generation, a fine texture with regional differences within the affected myocardium can be assumed.[32] Interestingly, another Teta feature (ie, Teta1) has been recently implicated to allow for the diagnosis of MI on non–contrast-enhanced cardiac cine MR images in the absence of visually detectable signal abnormalities.[14]

The following study limitations must be acknowledged. First, this was a retrospective study with inherent limitations. Second, TA was limited to a single image of interest. Third, we included only a relatively low number of patients and controls, especially when considering a machine learning-based approach.

Larger data sets are likely to improve the performance of supervised classifiers and would further decrease overfitting of the algorithms. Finally, we performed TA on CT DICOM images obtained from a single scanner to reduce feature interscanner noise as proposed by Mackin et al,[33] similarly our image reconstruction is unique to a single vendor. Thus, generalizability of our results needs to be proven by future studies including different CT machines, as well as different corresponding image reconstruction algorithms.

In conclusion, our study indicates promising results of TA and machine learning for detecting acute or chronic MI on non–contrast-enhanced low-dose CCT images. Certainly, findings need to be validated in future prospective trials including a larger sample size.

REFERENCES

1. von Ballmoos MW, Haring B, Juillerat P, et al. Meta-analysis: diagnostic performance of low-radiation-dose coronary computed tomography angiography. *Ann Intern Med*. 2011;154:413–420.
2. Leipsic J, Taylor CM, Gransar H, et al. Sex-based prognostic implications of nonobstructive coronary artery disease: results from the international multicenter CONFIRM study. *Radiology*. 2014;273:393–400.
3. Nikolaou K, Knez A, Sagmeister S, et al. Assessment of myocardial infarctions using multidetector-row computed tomography. *J Comput Assist Tomogr*. 2004; 28:286–292.
4. Gosalia A, Haramati LB, Sheth MP, et al. CT detection of acute myocardial infarction. *AJR Am J Roentgenol*. 2004;182:1563–1566.
5. Agatston AS, Janowitz WR, Hildner FJ, et al. Quantification of coronary artery calcium using ultrafast computed tomography. *J Am Coll Cardiol*. 1990;15: 827–832.
6. Baron KB, Choi AD, Chen MY. Low radiation dose calcium scoring: evidence and techniques. *Curr Cardiovasc Imaging Rep*. 2016;9:12.
7. Liew G, Chow C, van Pelt N, et al. Cardiac Society of Australia and New Zealand Position Statement: coronary artery calcium scoring. *Heart Lung Circ*. 2017;26: 1239–1251.
8. Aerts HJ, Velazquez ER, Leijenaar RT, et al. Decoding tumour phenotype by noninvasive imaging using a quantitative radiomics approach. *Nat Commun*. 2014;5:4006.
9. Gillies RJ, Kinahan PE, Hricak H. Radiomics: images are more than pictures, they are data. *Radiology*. 2016;278:563–577.
10. Hainc N, Stippich C, Stieltjes B, et al. Experimental texture analysis in glioblastoma: a methodological study. *Invest Radiol*. 2017;52:367–373.
11. Ahn SY, Park CM, Park SJ, et al. Prognostic value of computed tomography texture features in non-small cell lung cancers treated with definitive concomitant chemoradiotherapy. *Invest Radiol*. 2015;50:719–725.
12. Pickles MD, Lowry M, Gibbs P. Pretreatment prognostic value of dynamic contrast-enhanced magnetic resonance imaging vascular, texture, shape, and size parameters compared with traditional survival indicators obtained from locally advanced breast cancer patients. *Invest Radiol*. 2016;51:177–185.
13. Hinzpeter R, Wagner MW, Wurnig MC, et al. Texture analysis of acute myocardial infarction with CT: First experience study. *PLoS One*. 2017;12:e0186876.
14. Baessler B, Mannil M, Oebel S, et al. Subacute and chronic left ventricular myocardial scar: accuracy of texture analysis on nonenhanced cine MR images. *Radiology*. 2018;286:103–112:170213.
15. Goetti R, Kozerke S, Donati OF, et al. Acute, subacute, and chronic myocardial infarction: quantitative comparison of 2D and 3D late gadolinium enhancement MR imaging. *Radiology*. 2011;259:704–711.
16. Cerqueira MD, Weissman NJ, Dilsizian V, et al. Standardized myocardial segmentation and nomenclature for tomographic imaging of the heart. A statement for healthcare professionals from the Cardiac Imaging Committee of the Council on Clinical Cardiology of the American Heart Association. *Int J Cardiovasc Imaging*. 2002;18:539–542.
17. Sabarudin A, Sun Z. Radiation dose measurements in coronary CT angiography. *World J Cardiol*. 2013;5:459–464.
18. Sogawa K, Nodera H, Takamatsu N, et al. Neurogenic and myogenic diseases: quantitative texture analysis of muscle US data for differentiation. *Radiology*. 2017;283:492–498:160826.
19. Szczypinski PM, Strzelecki M, Materka A, et al. MaZda—a software package for image texture analysis. *Comput Methods Programs Biomed*. 2009;94:66–76.
20. Collewet G, Strzelecki M, Mariette F. Influence of MRI acquisition protocols and image intensity normalization methods on texture classification. *Magn Reson Imaging*. 2004;22:81–91.
21. Landis JR, Koch GG. The measurement of observer agreement for categorical data. *Biometrics*. 1977;33:159–174.
22. Zhang X, Yan LF, Hu YC, et al. Optimizing a machine learning based glioma grading system using multi-parametric MRI histogram and texture features. *Oncotarget*. 2017;8:47816–47830.
23. Juntu J, Sijbers J, De Backer S, et al. Machine learning study of several classifiers trained with texture analysis features to differentiate benign from malignant soft-tissue tumors in T1-MRI images. *J Magn Reson Imaging*. 2010;31:680–689.
24. Sharma V, Singh S. CFS-SMO based classification of breast density using multiple texture models. *Med Biol Eng Comput*. 2014;52:521–529.
25. Dobbin KK, Simon RM. Optimally splitting cases for training and testing high dimensional classifiers. *BMC Med Genomics*. 2011;4:31.
26. Aha DW, Kibler D, Albert MK. Instance-based learning algorithms. *Machine Learning*. 1991;6:37–66.
27. Atkeson CG, Moore AW, Schaal S. Locally weighted learning. *Artif Intell Rev*. 1997;11:11–73.
28. Taylor AJ, Cerqueira M, Hodgson JM, et al. ACCF/SCCT/ACR/AHA/ASE/ASNC/NASCI/SCAI/SCMR 2010 Appropriate Use Criteria for Cardiac Computed Tomography. A Report of the American College of Cardiology Foundation Appropriate Use Criteria Task Force, the Society of Cardiovascular Computed Tomography, the American College of Radiology, the American Heart Association, the American Society of Echocardiography, the American Society of Nuclear Cardiology, the North American Society for Cardiovascular Imaging, the Society for Cardiovascular Angiography and Interventions, and the Society for Cardiovascular Magnetic Resonance. *J Cardiovasc Comput Tomogr*. 2010;4:407.e1–407.e33.
29. Ma Y, Zhu L. A review on dimension reduction. *Int Stat Rev*. 2013;81:134–150.
30. Depeursinge A, Chin AS, Leung AN, et al. Automated classification of usual interstitial pneumonia using regional volumetric texture analysis in high-resolution computed tomography. *Invest Radiol*. 2015;50:261–267.
31. Materka A. Texture analysis methodologies for magnetic resonance imaging. *Dialogues Clin Neurosci*. 2004;6:243–250.
32. Mayerhoefer ME, Szomolanyi P, Jirak D, et al. Effects of magnetic resonance image interpolation on the results of texture-based pattern classification: a phantom study. *Invest Radiol*. 2009;44:405–411.
33. Mackin D, Fave X, Zhang L, et al. Measuring computed tomography scanner variability of radiomics features. *Invest Radiol*. 2015;50:757–765.